Electronic Supplementary Material (ESI) for Chemical Communications

Supplementary Information

Controlled anion exchange strategy to synthesize Bi_2S_3 nanocrystals/BiOCl hybrid architectures with efficient visible light photoactivity

Hefeng Cheng, Baibiao Huang*, Xiaoyan Qin, Xiaoyang Zhang and Ying Dai

Experimental Section

Preparation: The BiOCl hierarchical architectures were prepared by an ion liquid-assisted solvothermal method. Briefly, $Bi(NO_3)_3 \cdot 5H_2O$ (0.97 g) and 1-dodecyl-3-methylimidazolium chloride ($[C_{12}Mim]Cl$, 0.86 g) were separately dissolved in 40 mL of 2-methoxyethanol and mixed together. The suspension was stirred and transferred into a 100 mL autoclave. The autoclave was heated and maintained at 160 °C for 2 h and cooled down to room temperature. The product was collected, washed, and dried in vacuum.

For synthesis of the Bi_2S_3 NCs/BiOCl hybrid, the prepared BiOCl sample (0.260 g) was introduced to the three different aqueous solutions containing thiourea (0.075 g), cysteine (0.122 g) and thiacetamide (TAA, 0.075 g) with constant stirring for 2–4 h at room temperature (RT), respectively. In addition, the BiOCl sample was also suspended in another aqueous solution containing TAA treated at elevated temperature (60 °C) with other experimental conditions unchanged.

For comparison, bulk Bi_2S_3 was prepared by reacting stoichiometric $Bi(NO_3)_3$ and TAA in ethylene glycol at 160 °C for 12 h. The reference photocatalyst N-doped P25 was prepared according to the method previously reported.[1]

Characterization: Powder X-ray diffraction (XRD) patterns were recorded on a Bruker AXS D8 advance powder diffractometer (Cu Kα X-ray radiation, λ = 0.154056 nm). Raman spectra were measured on Horiba LabRAM HR system with laser excitation of 532 nm. The scanning electron microscopy (SEM) images were obtained on a Hitachi S-4800 microscope with an accelerating voltage of 7.0 kV. The chemical

element mapping and energy-dispersive X-ray spectrum (EDS) were examined by an energy dispersive X-ray spectrometer equipped in the SEM machine. The transmission electron microscopy (TEM) and high resolution TEM (HRTEM) images were performed by a JEOL JEM-2100 instrument. UV–Vis diffuse reflectance spectra were collected on a Shimadzu UV 2550 recording spectrophotometer, which was equipped with an integrating sphere. The N_2 sorption properties were determined on a Micromeritics ASAP 2020 apparatus at liquid nitrogen temperature.

Photocatalytic evaluation: The photocatalytic performances of the as-prepared products were evaluated by decomposition of 2,4-dichlorophenol (2, 4-DCP) and methyl orange (MO) under visible light irradiation at room temperature. A 300 W Xe arc lamp (PLS-SXE300, Beijing Trusttech Co., Ltd.) was used as the light source and equipped with an ultraviolet cutoff filter to provide visible light ($\lambda \geq 400$ nm). The distance between the liquid surface of the suspension and the light source was set about 10 cm. The photocatalytic experiments were performed with the sample powder (100 mg) suspended in 2,4-DCP or MO (20 mg L^{-1}, 100 mL) with constant stirring. Prior to irradiation, the suspensions were stirred in the dark for 1 h to insure the adsorption/desorption equilibrium. At the given time intervals, about 5 ml of the suspension was taken for the following analysis after centrifugation. The 2,4-DCP and MO photodecomposition were then analyzed at 284 and 464 nm, respectively, as a function of irradiation time on a UV–Vis spectrophotometer (Shimadzu UV 2550).

[1] K. Maeda, Y. Shimodaira, B. Lee, K. Teramura, D. Lu, H. Kobayashi and K. Domen, *J. Phys. Chem. C*, 2007, **111**, 18264.

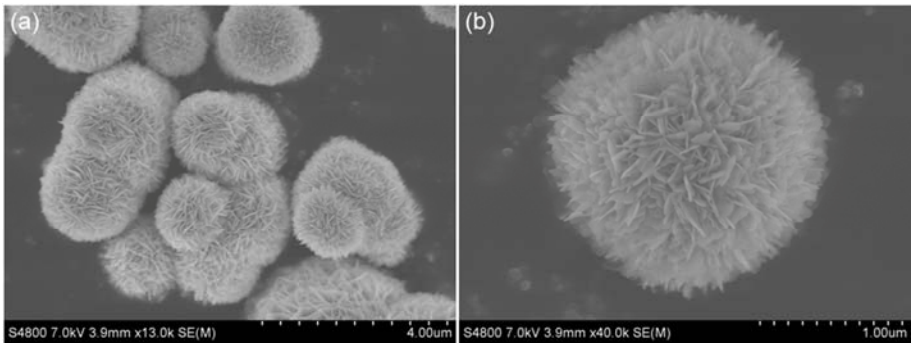

Fig. S1 SEM images of the as-prepared BiOCl hierarchical microspheres.

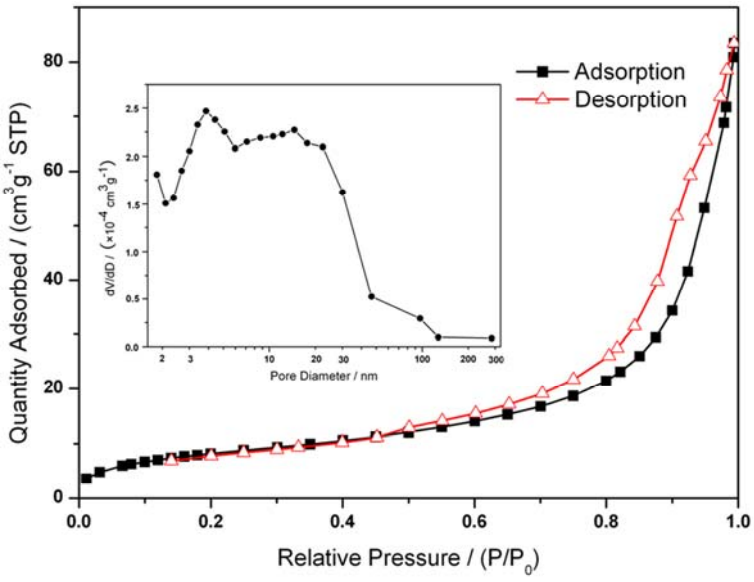

Fig. S2 N_2 adsorption–desorption isotherm plot and corresponding pore-size distribution (insert) of as-prepared BiOCl hierarchical architectures.

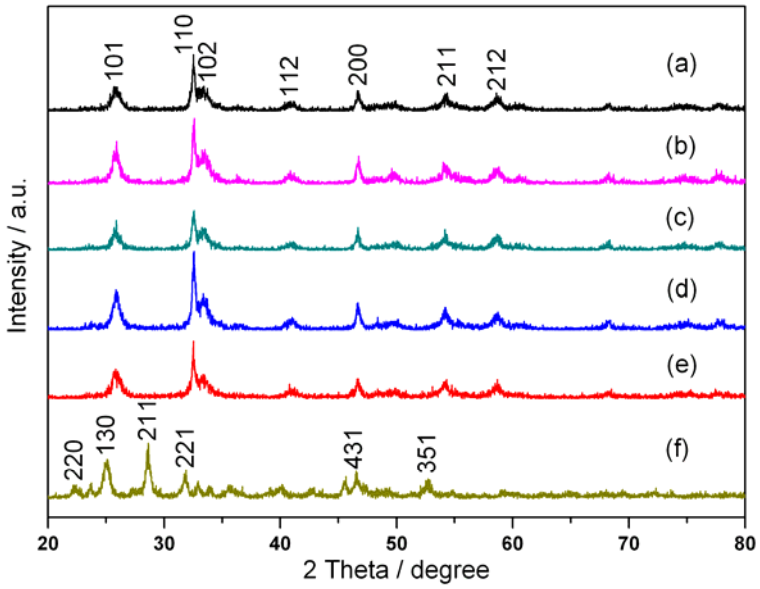

Fig. S3 XRD patterns of the as-prepared samples: (a) BiOCl, (b-e) Bi_2S_3 NCs/BiOCl hybrids prepared under thiourea, cysteine, TAA, and TAA at 60 °C conditions, respectively; (f) bulk Bi_2S_3.

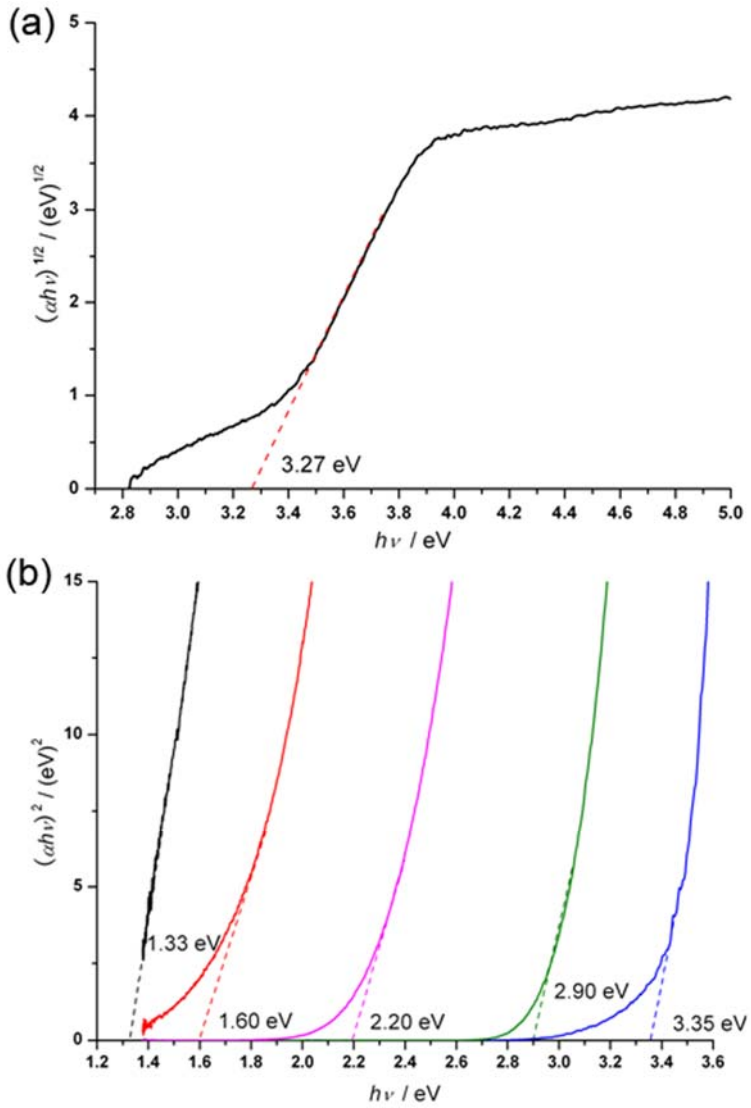

Fig. S4 (a) The plot of $(\alpha h\nu)^{1/2}$ versus $(h\nu)$ for BiOCl and (b) the plots of $(\alpha h\nu)^2$ versus $(h\nu)$ for Bi_2S_3 and Bi_2S_3 NCs/BiOCl hybrid materials.

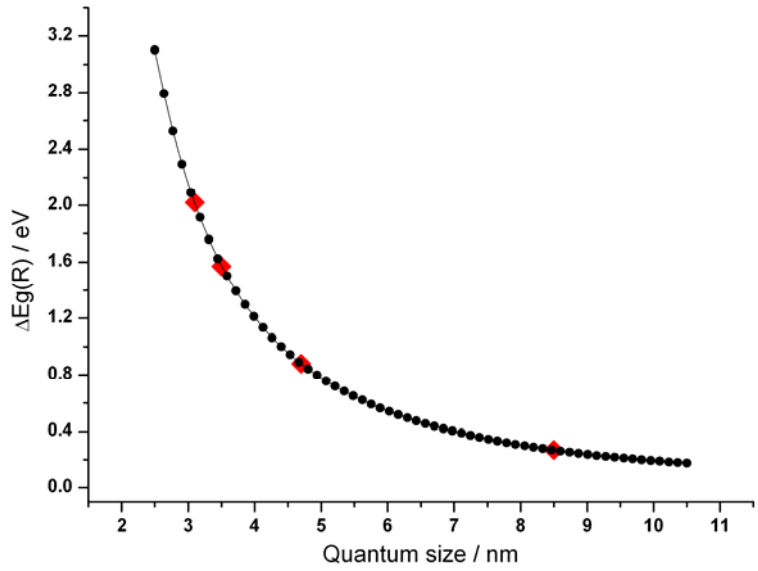

Fig. S5 The relationship between band gap shift $\Delta E_g(R)$ and the crystal radius R.

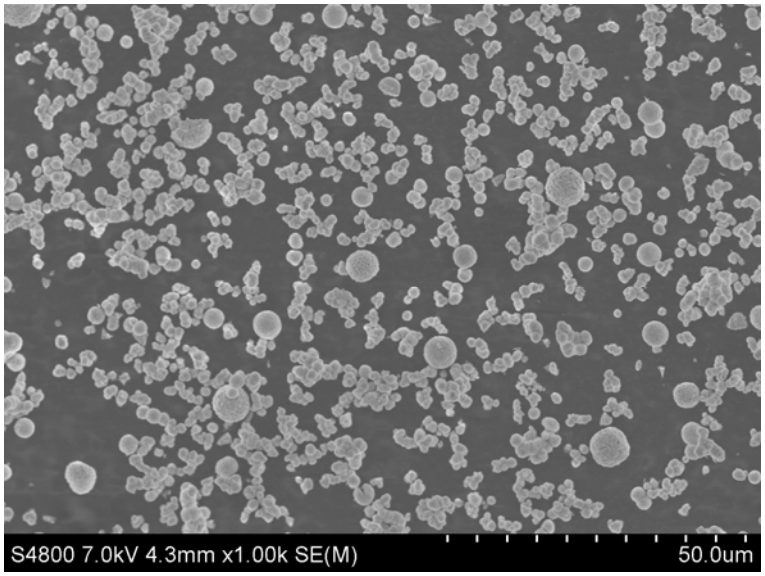

Fig. S6 A typical overall SEM image of the as-prepared Bi_2S_3/BiOCl hybrid architectures.

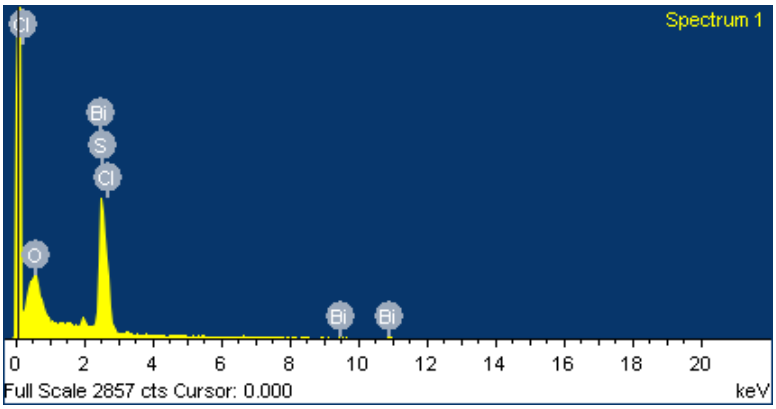

Element	Weight%	Atomic%
O K	7.88	41.04
S K	0.12	0.31
Cl K	11.24	26.43
Bi M	80.77	32.22
Totals	100.00	

Fig. S7 EDS spectrum and detailed information about the composition of Bi_2S_3 NCs/BiOCl hybrid synthesized using TAA as the sulfur source at room temperature.

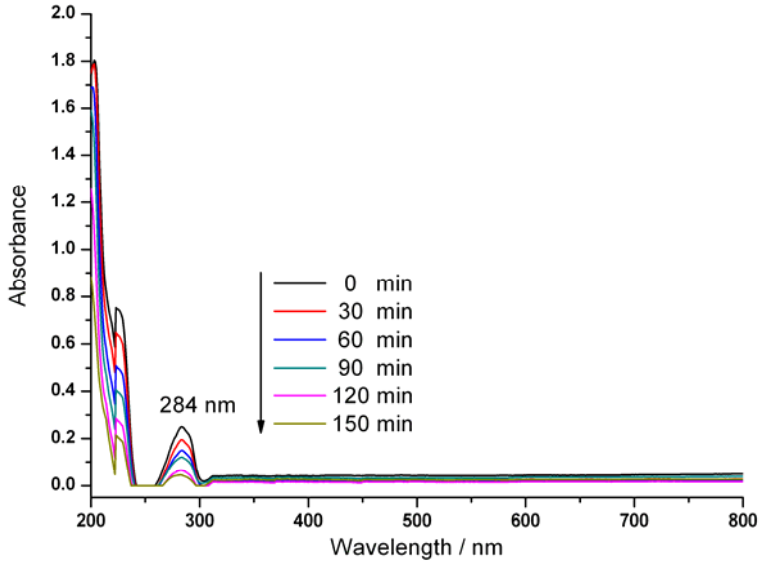

Fig. S8 The absorption spectra changes of 2,4-DCP solution in the presence of Bi_2S_3 NCs/BiOCl hybrid architectures synthesized using TAA as sulfur source at room temperature under visible light irradiation.

Photocatalytic degradation of MO dye solution

The photocatalytic activities of the hybrids were also carried out by degradation of methyl orange (MO) dye in solution under visible light irradiation ($\lambda \geq 400$ nm). Prior to irradiation, the suspensions were stirred in the dark for 1 h to ensure the adsorption–desorption equilibrium. As shown in Fig. S9, the Bi_2S_3 NCs/BiOCl hybrid shows an adsorption capacity of 22.1%, which would merely stem from the physical adsorption. The absorption spectra changes of MO dye solution in the presence of Bi_2S_3 NCs/BiOCl hybrid was presented in Fig. S10, and MO dye was greatly degraded. Though bulk Bi_2S_3 absorbs the light across the entire visible range, no MO degradation was observed on the bulk Bi_2S_3 catalyst, probably due to the fast recombination of the photoexcited carriers. BiOCl could degrade 35.4% of MO dye molecules, which could originate from the photosensitization process. As a reference photocatalyst, N-doped P25 could only degrade 9.8% of MO dye molecules. In the case of Bi_2S_3 NCs/BiOCl hybrid, the photocatalytic degradation can reach as high as 75.3% in 90 min under visible irradiation (Fig. S10). Given that the photodegradation always follows the pseudo-first-order, MO degradation rate over the Bi_2S_3 NCs/BiOCl hybrid (0.931 h^{-1}) is faster than that of N-doped P25 (0.069 h^{-1}) by a factor of thirteen. In addition, the relationship between Bi_2S_3 quantum sizes and the photocatalytic performances of Bi_2S_3 NCs/BiOCl hybrid was also investigated (Fig. S12). It is found that the 4.7 nm Bi_2S_3 NCs/BiOCl hybrid exhibits the best photocatalytic performance.

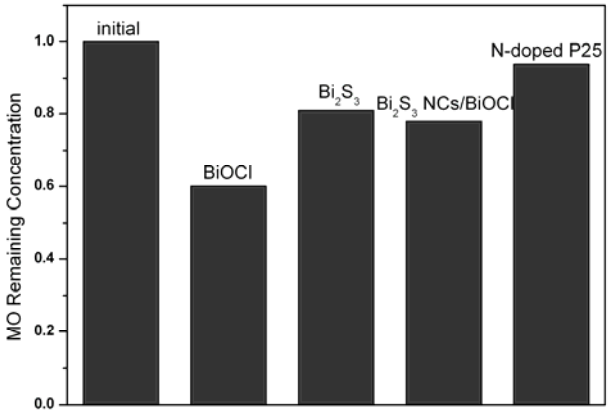

Fig. S9 The bar plot illustrating the remaining concentration of MO over different photocatalysts after adsorption/desorption equilibrium in the dark.

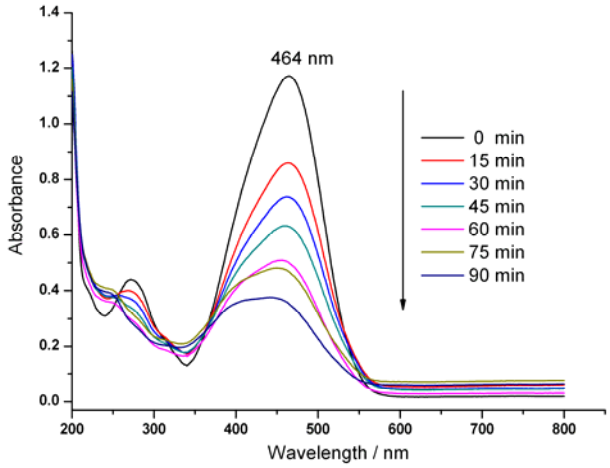

Fig. S10 The absorption spectra changes of MO dye solution in the presence of Bi_2S_3 NCs/BiOCl hybrid architectures synthesized using TAA as sulfur source at room temperature under visible light irradiation.

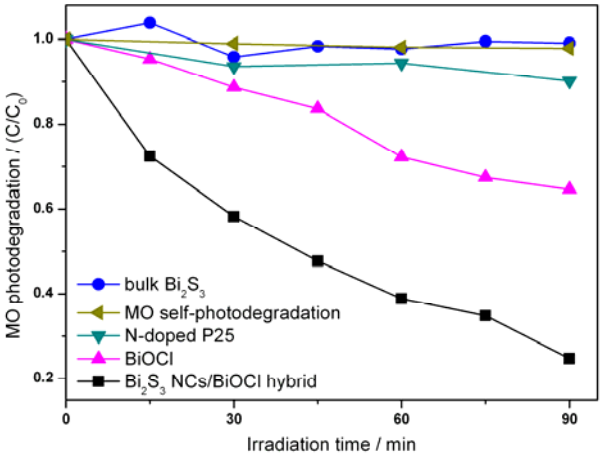

Fig. S11 Photodegradation of MO dye solution with time over different photocatalysts under visible irradiation.

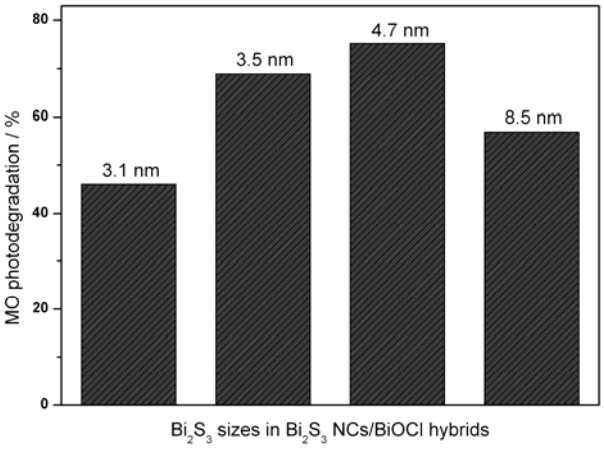

Fig. S12 The influences of Bi_2S_3 sizes to the MO photocatalytic degradation of Bi_2S_3 NCs/BiOCl hybrid.

Band position calculations

For an inorganic semiconductor, the valence band (VB) position at the point of zero charge can be calculated by the following empirical formula [1]:

$$E_{VB} = X - E^e + 0.5E_g \qquad (2)$$

where X is the absolute electronegativity of the semiconductor, which is defined as the geometric mean of the absolute electronegativity of the constituent atoms, E^e is the energy of free electrons on the hydrogen scale (*ca.* 4.5 eV), E_{VB} is the VB edge potential and Eg is the band gap of the semiconductor. The conduction band (CB) position can be deduced by $E_{CB} = E_{VB} - E_g$. The calculated band positions of bulk Bi_2S_3, BiOCl and BiOBr are summarized in **Table S1**.

Table S1. Band energy positions of bulk Bi_2S_3, BiOCl and BiOBr.

semiconductors	electronegativity (X)	estimated E_g (eV)	calculated VB position (eV) *vs.* NHE	calculated CB position (eV) *vs.* NHE
Bulk Bi_2S_3	5.273	1.33	1.438	0.108
BiOCl	6.360	3.27	3.495	0.225
BiOBr	6.176	2.7	3.026	0.326

[2] Y. Xu and M. A. A. Schoonen, *Am. Mineral.*, 2000, **85**, 543.

Extension to BiOBr

The above study has demonstrated that photocatalysis can be greatly improved by surface sensitization. As an extension, Bi_2S_3 NCs/ BiOBr architecture hybrid was also prepared by partial anion exchange between BiOBr architecture and TAA at room temperature (see the Supporting Information). Owing to the quantum confinement of Bi_2S_3 NCs, the Bi_2S_3 NCs/ BiOBr architecture hybrid shows strong visible light absorption and the absorption edge shifts to about 600 nm (Figure S6). In addition, the hybrid displays highly improved photocatalytic activity in photodegradation of MO dye, which is much higher than BiOBr sample (Figure S7). Analogous to BiOCl, BiOBr ($a = b = 0.392$ nm, $c = 0.808$ nm) could adopt a topotactic transformation into Bi_2S_3 by anion exchange with TAA. The lateral dimension difference between BiOBr and Bi_2S_3 is 1.53 %, which is smaller than that of BiOCl and Bi_2S_3 (2.52 %).

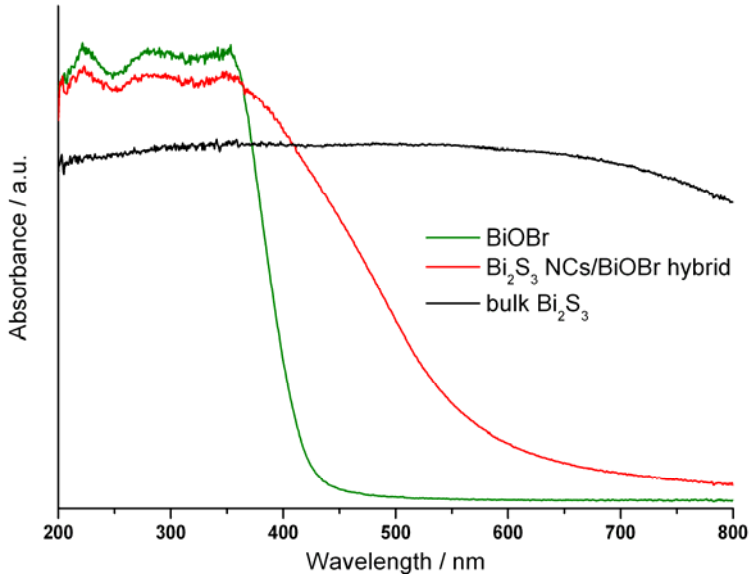

Fig. S13 UV–vis diffuse reflectance spectra of the samples.

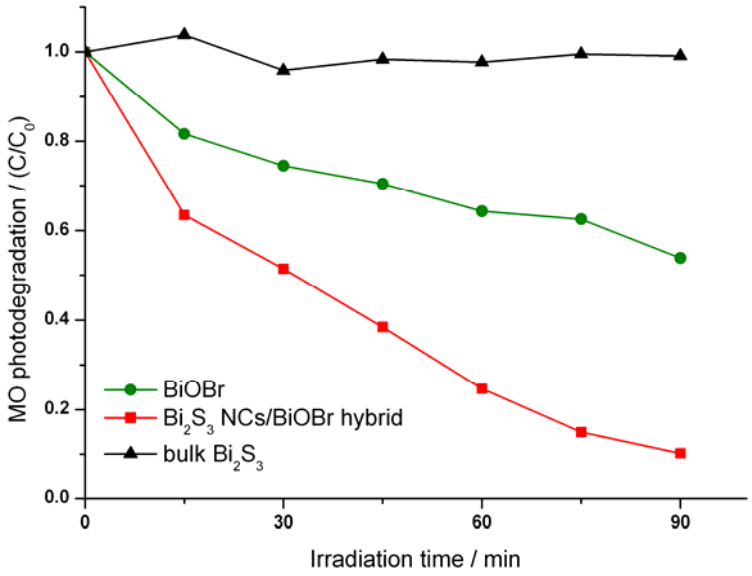

Fig. S14 Photocatalytic degradation of MO dyes over different samples under visible light irradiation ($\lambda \geq 400$ nm).